ACS SENSORS

Article

Cite This: ACS Sens. 2020, 5, 140−146

pubs.acs.org/acssensors

Immunoglobulin G-Based Steric Hindrance Assay for Protein Detection

Yifan Dai,[†,‡] Wei Xu,[§] and Chung Chiun Liu*[,†,‡]

[†]Electronics Design Center, [‡]Department of Chemical and Biomolecular Engineering, and [§]Department of Biomedical Engineering, Case Western Reserve University, Cleveland 44106, Ohio, United States

Supporting Information

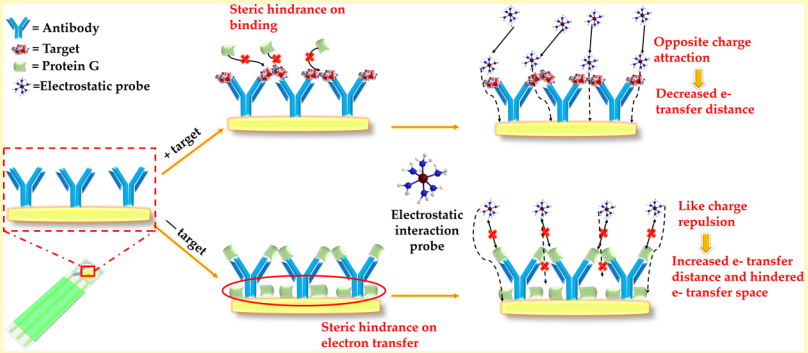

ABSTRACT: With the imminent needs of rapid, accurate, simple point-of-care systems for global healthcare industry, electrochemical biosensors have been widely developed owing to their cost-effectiveness and simple instrumentation. However, typical electrochemical biosensors for direct analysis of proteins in the human biological sample still suffer from complex biosensor fabrication, lack of general method, limited sensitivity, and matrix-caused biofouling effect. To resolve these challenges, we developed a general electrochemical sensing strategy based on a designed steric hindrance effect on an antibody surface layer. This strategy utilizes the interaction pattern of protein-G and immunoglobulin G (Fc and Fab regions), providing a steric hindrance effect during the target capturing process. The provided steric hindrance effect minimizes the matrix effect-caused fouling surface and altered the path of electron transfer, delivering a low-fouling and high-sensitivity detection of protein in complex matrices. Also, an enzyme-based horseradish peroxidase/hydroquinone/H_2O_2 transduction system can also be applied to the system, demonstrating the versatility of this sensing strategy for general electrochemical sensing applications. We demonstrated this platform through the detection of Tau protein and programming death ligand 1 with a subpico molar detection limit within 10 min, satisfying the clinical point-of-care requirements for rapid turnaround time and ultrasensitivity.

KEYWORDS: *steric hindrance, electrochemical biosensor, protein G, antibody-based detection, protein detection*

Downloaded via UNIV OF EXETER on July 17, 2020 at 07:13:19 (UTC).
See https://pubs.acs.org/sharingguidelines for options on how to legitimately share published articles.

The development of a simple, accurate, efficient point-of-care biosensing platform is critical for global health, especially for frequent evaluation of drug treatments and miscellaneous diseases diagnostics in developing areas.[1,2] However, current biomarker quantification approaches, such as ELISA and Western Blots, remain to be complexly operated, time-consuming, and expensive processes,[3,4] which cannot satisfy the imminent needs for worldwide disease diagnostics. Recent progress in electrochemistry-based biosensors has demonstrated the possibility to achieve a rapid, accurate, cost-effective platform for biomolecular quantifications.[5−9] Hence, electrochemical biosensing platform has been widely developed for detection of a wide categories of analytes, such as nucleic acids, proteins, and cells.[9−13] However, because of the complexity of the surface chemistry (involving the biomolecule binding reaction and the following electrochemical quantification) and the lack of general methods for electrochemical biosensor construction, most of the current electrochemical biosensors still suffer from complicated preparation procedure, limited analytical sensitivity, and high-fouling possibility. To overcome these limitations, we herein describe a novel, versatile, steric hindrance interaction-based electrochemical biosensing strategy for protein detection.

Application of steric hindrance effect on the biosensing platform has been demonstrated to be an effective means to enhance the biosensing performance.[14−16] Previous biosensor developments using steric hindrance effect typically apply a surface competing hybridization and binding design, using large macromolecules (such as antibody) to provide steric hindrance for DNA hybridization on a high density surface, which was able to detect small molecules and antibody.[14,15,17] Inspired by these designs, we herein describe a general protein detection strategy based on steric hindrance effect through a simple antigen−antibody binding interaction and a general

Received: September 27, 2019
Accepted: December 12, 2019
Published: December 12, 2019

© 2019 American Chemical Society

DOI: 10.1021/acssensors.9b01902
ACS Sens. 2020, 5, 140−146

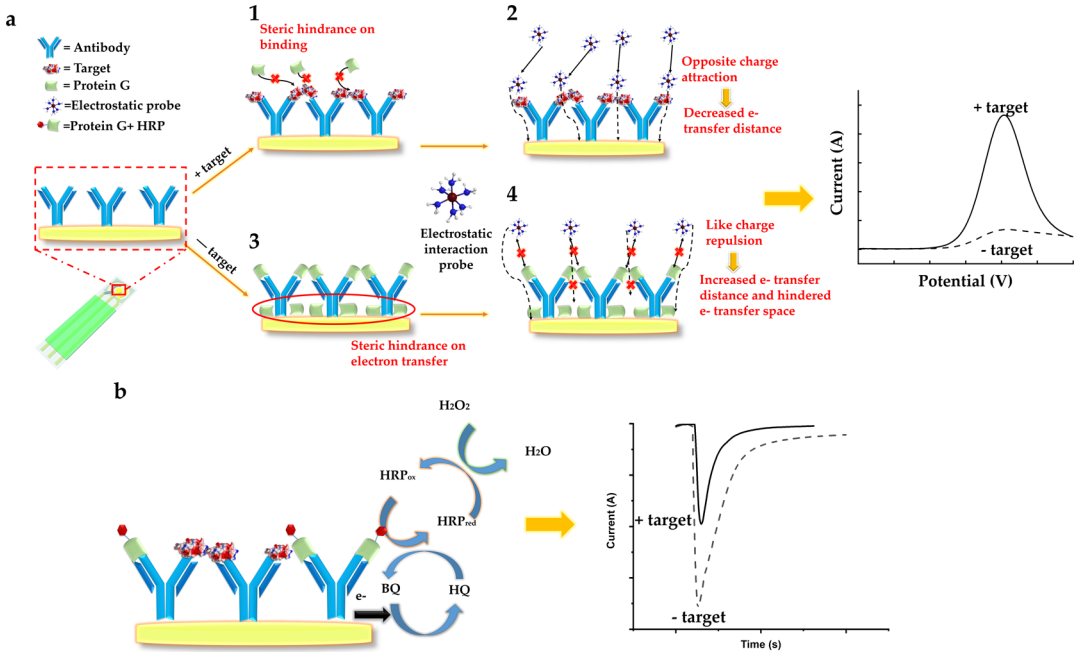

Figure 1. (a) Schematic illustration of the construction principle of steric hindrance effect using protein G−IgG antibody interaction pair. Electrochemistry-based electrostatic quantification of target protein through the difference in electron-transfer distance during the electrochemical reaction of the redox probe ($[Fe(CN)_6]^{3-/4-}$). (b) Illustration of the HRP-based enzymatic transduction method to quantify protein G concentration, which can be inversely correlated to the concentration of the target protein.

antibody binding protein to provide the steric hindrance effect. For protein-based biomarker detection, the corresponding immunoglobulin G (IgG) antibody is typically utilized as the recognition element. Therefore, an interaction element that can compete with the antibody−antigen interaction can be utilized to provide the steric hindrance effect. Moreover, a specific molecule that can generally interact with IgG antibody is desirable for a general protein detection strategy. Therefore, an IgG binding protein, protein G (containing two targeted binding sites at Fc region and Fab region of the IgG), is selected for providing the steric hindrance effect by interacting with IgG on the electrode surface during the antibody−antigen recognition process.[18,19] Also, the binding site of protein G for serum albumin is removed in order to eliminate nonspecific binding of protein G with human serum components. In general, this method provides a simple, low-fouling, general strategy for construction of protein biomarker detection interface.

RESULTS AND DISCUSSION

Principle of Detection. A three-electrode, vapor-deposited gold thin film sensor prototype was applied for the development of this biosensing strategy. The detailed configuration and characterization of this sensor prototype can be found in a previous study.[20] The principle that underlies the construction of protein detection surface for steric hindrance effect is shown in Figure 1. Specifically, in this study, Tau protein, a biomarker of neurodegenerative disorders, was first used as the detection target for the development.[21,22] The formation of the IgG antibody layer on the sensor surface is through a previous reported bioconjugation method to modify the antibody with an external thiol linker,[20] which directly physically absorbed onto the gold electrode. After the formation of the IgG antibody layer on the electrode, a fixed concentration of protein G is used as a competitor against the target (Tau protein) binding to the antibody during the sample incubation process. With the presence of the target, the enriched antigen−antibody complexes provide the steric hindrance effect for protein G binding to the Fc and Fab region (Figure 1a-1). Therefore, a clear space is provided for the electron tunneling process of the further electrochemical redox reaction for Tau quantification (Figure 1a-2), resulting in a high electrochemical current. Without the presence of the target, protein G occupies the Fab and Fc region of the antibody (Figure 1a-3), hindering the electron tunneling process of the electrochemical redox reaction (Figure 1a-4). Moreover, for Tau quantification, a previous demonstrated electrostatic interaction-based quantification method is applied, owing to the electrostatic attraction between the positive charge of Tau protein (pI = 8.6) and negative charge of the ferrocynaide redox at physiological testing condition (pH = 7.4).[23] From the electrostatic interaction perspective, protein G (pI = 4.6) is negatively charged and would repulse with negatively charged probe (Figure 1a-4), therefore further decreasing the current at low Tau concentration condition. Furthermore, in order to develop a generalizable sensing strategy disregarding the charge of the analyte, an enzymatic transduction strategy is also designed (Figure 1b). A horseradish peroxidase (HRP)-linked protein G is applied to offer the steric hindrance effect. Therefore, the amount of protein G bound can be quantified through the electrochemical enzymatic reaction of HRP/hydroquinone (HQ)/H_2O_2 system to inversely indicate the target concentrations.[24] We verified the enzymatic transduction platform through the detection of programing death ligand 1 (PD-L1), a predictive biomarker for nonsmall cell lung cancer.[25] In general, this simple antibody-based steric hindrance sensing strategy can be diversely applied for the detection of protein biomarkers.

DOI: 10.1021/acssensors.9b01902
ACS Sens. 2020, 5, 140−146

Optimizing Antibody Surface Packing Density. In order to provide the steric hindrance effect, it is crucial to optimize the surface antibody packing density, providing sufficient spatial distance for protein G−antibody binding interactions. We first evaluated the ideal packing density of surface antibody layer essential for the intercalation process of redox couple for electrostatic interaction as shown in Figure 2a. Different concentrations of bioconjugated antibody were applied for incubation of 90 min to deliver different surface antibody densities. After the incubation process, $[Fe(CN)_6]^{3-/4-}$was used to test the surface resistance variation by differential pulse voltammetry (DPV) at pH = 7.2 (isoelectric point of the Tau antibody, therefore preventing any electrostatic interaction between the antibody and the probe). As shown in Figure 2a, the redox current outputs at antibody concentrations of 0.16−3.2 nM demonstrated a linear decay correlation (R^2 = 0.972) with the increasing surface density. However, for antibody concentration over 3.2 nM, a significant decrease of current output was observed, falling out of the linear decay range of the previous impedance behavior. This phenomenon can be explained as that under an ideal antibody packing density, sufficient space is available for redox probe migrating into the antibody layer (Figure 2a-1). Therefore, during the electrochemical reaction, redox probe has a shorter electron tunneling distance, leading to a higher current output. Nevertheless, at a high incubation concentration of the antibody, the formation of a dense antibody layer blocks the migration of the redox probe (Figure 2a-2). The electron tunneling distance is significantly increased, therefore decreasing the electrochemical reaction kinetic significantly. To further prove this theory, we tested the same antibody cover density by varying the pH value of the DPV testing environment to 6.2. Based on the isoelectric point of this antibody tested by zeta-potential, it should be positively charged at pH < 7.22. Therefore, the electrostatic attraction performance was observed under the ideal surface packing condition as shown in Figure S1, confirming that the sufficient space was provided by the ideal surface density range. Hence, a concentration range (<3.2 nM) was selected for antibody incubation and further evaluations of the biosensing performance. After recognizing the antibody concentration range for the electrochemical test, to provide the steric hindrance effect, the packing density of antibody was further evaluated to deliver a suitable space for intercalation of protein G into the antibody Fc region. Under an ideal antibody density on the electrode surface as shown in Figure 2b-1, Fc region-linked protein G would significantly impede the electron-transfer process, therefore discriminating the sample with low abundance of target from the sample with a high abundance of target. We tested different antibody packing densities with incubation of 20 μL of a fixed concentration of protein G (100 nM) for 10 min to evaluate the DPV current change of the redox probe electrochemical reaction before and after the incubation of protein G onto the antibody layer. As shown in Figure 2b, a significant decrease of current was observed when surface antibody concentrations were lower than 0.80 nM. This phenomenon can be interpreted as that when surface antibody concentration was higher than 0.80 nM, there was not enough space for protein G to transfer into the Fc region part to complete the surface blocking. Therefore, with only Fab region binding sites occupied, similar impedance difference (presented by the change of current) was observed based on the nonideal surface packing condition as shown in Figure 2b-2. However, when the surface concentration of antibody was lower than 0.80 nM, ideal packing condition was achieved with sufficient space created for protein G to bind the Fc region of IgG and further blocked the electron transfer during the redox reaction, therefore leading to a substantial change of current.

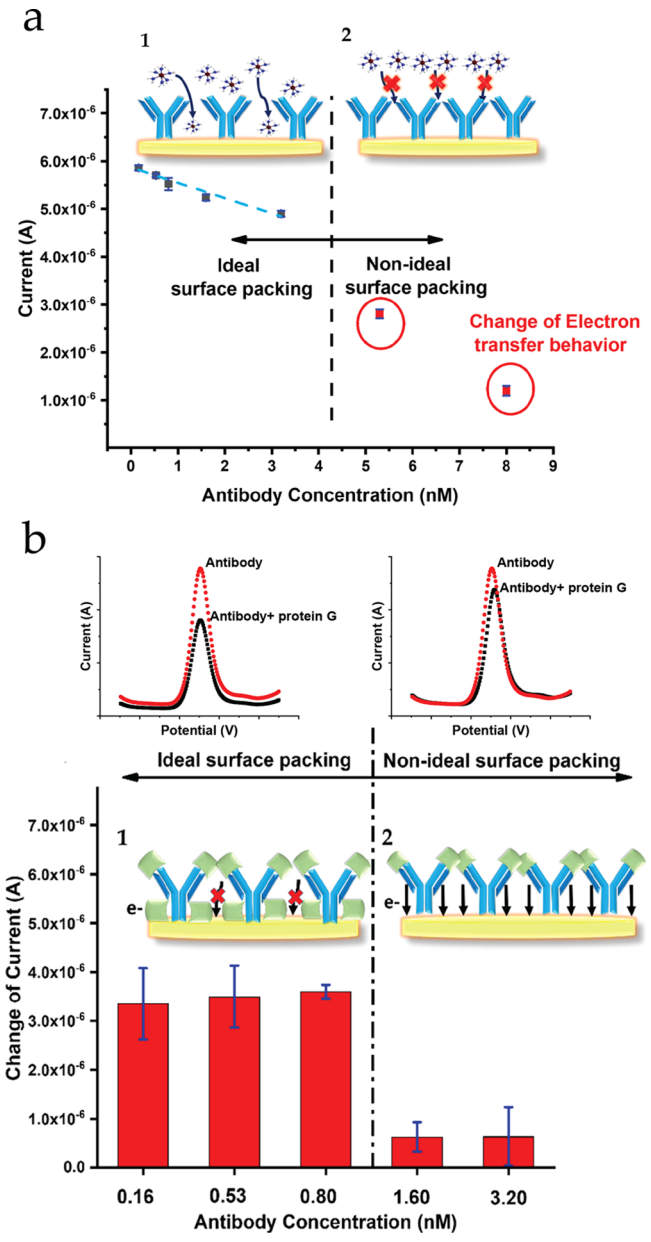

Figure 2. (a) DPV current outputs (n = 3) based on $[Fe(CN)_6]^{3-/4-}$ reaction for the optimized antibody surface density providing an ideal electrostatic interaction environment. (b) Evaluation of change of current outputs based on DPV with $[Fe(CN)_6]^{3-/4-}$ (n = 3) before and after introduction of protein-G into different concentrations of antibody prepared electrodes.

Electrostatic Detection of Tau Protein by Accumulated Charge (*Q*). After optimization of surface antibody density, we first tested the detection performance of the proposed system in 0.1 M phosphate-buffered saline (PBS) buffer solution. To evaluate the dynamic detection range, cathodic stripping analysis was firstly applied to evaluate the amount of surface antibody density based on the Au−S bond.[26] The immobilized antibody density was calculated to

DOI: 10.1021/acssensors.9b01902
ACS Sens. 2020, 5, 140−146

be at 44 pmol/mm^2 (Figure S2); therefore, a concentration range of Tau protein from picomolar level to femtomolar level in 20 μL solution was applied to evaluate the designed biosensing strategy. Electrochemical impedance spectroscopy (Text S2) was first conducted to verify the proposed steric hindrance construction based on the protein G−IgG interaction pair. Selected concentrations of Tau protein and a fixed concentration of protein G (100 nM) were co-incubated onto the sensor in order to evaluate whether the addition of Tau protein would compete the binding process with protein G. As shown in Figure 3, with the addition of

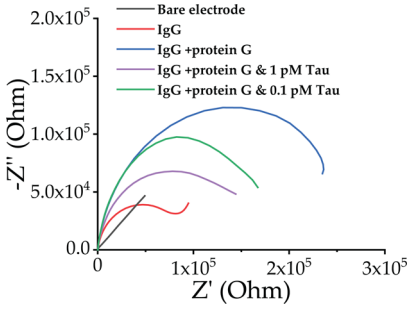

Figure 3. Electrochemical impedance spectroscopy using $[Fe(CN)_6]^{3-/4-}$ to evaluate the surface impedance variation caused by the addition of IgG (red), protein G (blue), and different concentrations (1 and 0.1 pM) of Tau protein (purple and green).

protein G only (blue), the impedance on the surface was significantly increased comparing with the impedance of only IgG (red). However, with the increasing concentration of Tau protein, the surface impedance was decreased (green and purple). This phenomenon can be explained as that the presence of Tau protein competed with protein G for the Fab binding sites; therefore, more $[Fe(CN)_6]^{3-/4-}$ probes were electrostatically attracted closer to the electrode. Subsequently, during the electrochemical reaction, electron tunneling kinetics was increased on the sensor surface, leading to a smaller surface impedance. The above observations verified the steric hindrance model we proposed.

DPV was then conducted with $[Fe(CN)_6]^{3-/4-}$ for electrostatic quantification of Tau protein. The sample DPV detection results are shown in Figure S2. Instead of using peak current output as the quantification signal for the target, we noticed that through integration of the charge (Q) accumulated under the DPV area actually provided a more precise and differentiated way for quantification of various concentrations as shown in Table 1. Specifically, to calculate the charge accumulated in the DPV test, we firstly transformed the potential axis (x-axis) into a time axis through potential increment and pulse width of DPV. Then, the charge accumulated between the detection curve and the base line (gray area) was integrated based on $dQ = di \times dt$ (Figure S3). As shown in Table 1, the average change for signal gradient by using the accumulated charge was higher than that of current peaks, indicating that using charge as transduction signal is a more sensitive and higher-resolution presentation for electrochemical quantification results. This phenomenon can be explained as that the peak current is typically a result of accumulation of charge inside the time frame of the differential pulse voltammetry. However, various concentrations of targets on the biosensor surface not only affected the kinetic of electrochemical reaction (indicated by the limiting/peak current) but also initiated different mass transport process of the electrochemical probe (indicated by the increase of overpotential), therefore resulting differences in the DPV E-I shape. Hence, to incorporate the concentration effect on mass transport to provide a more accurate characterization system, we let "charge" take in charge for the quantification (Figure S3).

As shown in Figure 4a, the charge accumulated was positively correlated with the concentration of Tau protein owing to the electrostatic interaction between positively charged Tau protein and the anion probe (leading to a shorter electron tunneling distance therefore faster reaction kinetics). A linear calibration curve was obtained ($Y = 9.96 \times 10^{-6}X - 1.77 \times 10^{-7}$) with a R^2 value of 0.983 and relative standard deviation (RSD) at 3.02%. A detection range was observed across picomolar to femtomolar level with a detection limit at 1.90 fM. Based on the best of our knowledge, this is one of the lowest detection limit on electrochemical detection of protein. Moreover, we challenged this biosensing strategy by target quantification from complex human matrix. Because of the complexity of biological components in real biological samples, electrochemical biosensor suffered from loss of signal (caused by hindered diffusion in complex matrix) or generation of nonspecific signal (caused by nonspecific absorption onto the electrode surface), therefore leading to a high-possibility of false positive/negative results. With the incorporation of protein G for providing the steric hindrance effect, this biosensing strategy was applied for the evaluation of performance on analysis of real human biological samples. Biological samples were first processed as shown in the Method section. The concentration of Tau protein in the human serum samples was analyzed through the biosensing system. Figure S4 presents the detection response using electrostatic interaction method after 5 min of sample incubation (same processing methods for PBS samples). Comparing with the detection performance in buffer solution, the direct analysis of serum sample showed around 20% decrease of signal. Owing to the positive correlation between target concentration and signal output by electrostatic interaction quantification method, as shown in Figure S4, no increase of signal was observed, indicating that there was limited nonspecific absorption happening in this system. Therefore, we suspected that the decrease of signal was mainly contributed by hindered diffusion due to the complexity of the matrix components. To minimize the hindered diffusion effect, we increased the

Table 1. Percentages of Signal Change Based on Concentration Differences Were Compared between Quantification through Charge Accumulated and Quantification through Peak Current[a]

concentration difference (fM)	3750−1875	1875−469	469−37	37−3.7	3.7−1.9	average % change
signal change by quantifying through Q	21.2%	33.3%	37.5%	58.2%	54.9%	**41.0%**
signal change by quantifying through i	11.6%	40.9%	47.8%	19.5%	32.4%	30.4%

[a]The calculation was based on % = (result 2 − result 1)/result 1.

DOI: 10.1021/acssensors.9b01902
ACS Sens. 2020, 5, 140−146

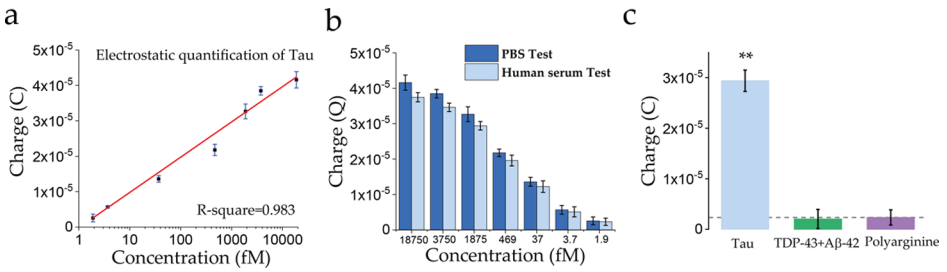

Figure 4. (a) Linear calibration curve of accumulated charge against different concentrations of Tau antigen covering the pico-to-femto molar range in buffer solution. (b) Comparison of signal outputs in different matrixes based on electrostatic quantification of Tau antigen. (c) Evaluation of the specificity for Tau detection using β-amyloid 42 (Aβ-42), TAR-DNA binding protein 43 (TDP-43) and polyarginine as nonspecific targets (**P < 0.01, vs nonspecific targets, gray dashed line indicating the RSD of the detection signal from zero concentration of Tau).

incubation time to 10 min for evaluation of the real biological sample. As shown in Figure 4b, with the increase of the incubation time, the matrix effect caused less than 10% of signal decrease, indicating an excellent low-fouling property of this platform. Also, the detection limit in human serum maintained at a femtomolar level. At the low concentration detection range, almost 100% signal was recovered comparing with that of the buffer test because at low concentration of target protein, high abundance of protein G performed better on blocking matrix proteins from attachment onto the electrode surface, demonstrating a low-fouling platform. It is worth mentioning that the total processing time including sample incubation was less than 15 min for this biosensing platform, delivering a rapid turnaround time for potential clinical application. Furthermore, the specificity of the detection platform was evaluated. The selectivity of the developed Tau protein biosensor was first examined by two other biomarkers of neurodegenerative disorders, β-amyloid 42 protein and TAR-DNA binding protein 43 (TDP-43).[27−29] The detection performance of sample with Tau concentration of 1875 fM and sample containing β-amyloid 42 protein (20 pM) and TAR-DNA binding protein 43 (50 pM) was compared (Figure 4c), demonstrating a high-significance of Tau detection over signal of nonspecific targets (P < 0.01). We also tested if these neurodegenerative biomarkers would interfere with the Tau target capture process by spiked sample with Tau and TDP-43 and Aβ-42 simultaneously. As shown in Figure S5, the detection signal of Tau was not interfered by coincubation with other relative protein markers. Moreover, we evaluated whether positively charged protein would become a signal interference by using polyarginine as a target, which also displayed insignificant signal. The average signal variation of these interference studies was around 2.1% (n = 3), which was within the RSD of the noninterference test, indicating the excellent selectivity of the antibody and the accuracy of this biosensing system.

Electrochemical Quantification through HRP/HQ/H_2O_2 System. In order to demonstrate the versatility of this sensing strategy, instead of quantifying the charge of the analyte, we can also quantify the protein G concentration using a HRP enzyme linked protein G to inversely indicate the concentration of Tau protein. Based on the different concentrations of surface captured HRP−protein G, the electrochemical signal was acquired using amperometric method at −0.2 V (vs Ag/AgCl) based on the enzymatic reaction.[24,30] As shown in Figure 5a, the current drop was plotted against the concentration of Tau antigen ($Y = 1.82 \times 10^{-4} - 3.37 \times 10^{-5}X$) with a R^2 value of 0.950 and RSD at

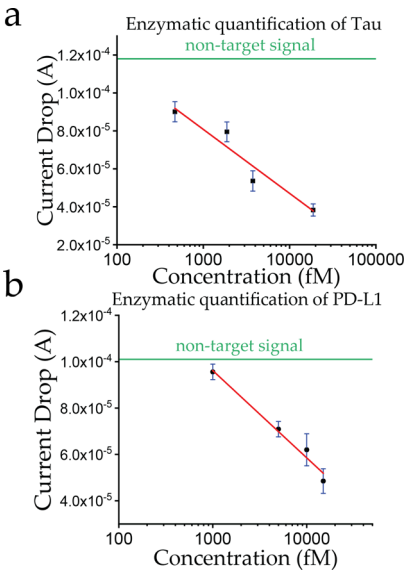

Figure 5. (a) Linear calibration curve of HRP enzymatic signal against Tau protein concentrations. (b) Linear calibration curve of HRP enzymatic signal PD-L1 protein concentrations. The green line represented the average signal acquired (n = 3) without the presence of the target.

6.2%. An experimental limit of detection was recognized at 469 fM using the enzymatic transduction method. The green line represents the average signal of three individual trails based on the signal acquired without target protein. We further evaluated the stability of the HRP/HQ/H_2O_2 transduction strategy on the response to a complex matrix. As shown in Figure S6, the matrix effect led to around 10% decay of current outputs by characterization of the amount of HRP−protein-G, which matched with the degree of signal loss based on characterization of Tau concentrations directly. We further challenged this enzymatic platform for the quantification of another protein target, PD-L1. As shown in Figure 5b, a dynamic detection range from sub pM to nM was achieved with a linear calibration curve of $Y = 2.09 \times 10^{-4} - 3.77 \times 10^{-5}X$ (R^2 = 0.989 and RSD = 4.8%). The current signal of enzymatic reaction acquired from protein G−HRP complex was comparable with that of Tau protein, indicating the generality of this biosensing strategy. However, higher detection limit was obtained comparing with that of Tau detection. We suspect that the difference of detection limit might due to the binding affinity difference of the antibody because the protein G signal actually went up at the picomolar concentration level of target for PD-L1, indicating that more

DOI: 10.1021/acssensors.9b01902
ACS Sens. 2020, 5, 140−146

protein G occupied the binding sites instead of the target. Overall, the inverse relationship between antigen concentration and protein G−HRP signal not only demonstrated the versatility of this biosensing platform construction method but also confirmed the detection principle of this novel strategy.

CONCLUSIONS

This electrochemical biosensing strategy demonstrates a highly sensitive, low-fouling platform through sterically hindered hybridization for the detection of protein biomarkers. The utilization of protein G and immunoglobulin G binding pair provides a general strategy for the construction of biosensing interface to deliver the steric hindrance effect. Highly sensitive electrostatic interaction method and enzyme-based electrochemical method were applied for signal transduction, demonstrating the versatility of this platform. The developed biosensing strategy was applied for the detection of human Tau protein and programming death ligand 1 with a sub picomolar sensitivity in 10 min. This robust, rapid biosensor construction strategy can be generally applied for antibody-based immunoassay development for the detection of protein-based biomarkers.

MATERIALS AND METHODS

Materials and Apparatus. Tau antibody, human Tau antigen, protein G, phosphate buffer saline, deionized water, ethylenedinitrilotetraacetic acid (EDTA), hydroxylamine hydrochloride, dimethyl sulfoxide, HQ, ferricyanide/ferrocyanide, and Amicon-10k tube were purchased from Sigma-Aldrich. Recombinant PD-L1 and anti-PD-L1 were purchased from Abcam. Sulfuric acid, nitric acid, potassium hydroxide, and *N*-succinimidyl *S*-acetylthioacetate were purchased from Thermo Fisher Scientific. A CHI 660C Electrochemical Workstation from CH Instrument, Inc., Austin, TX was used for electrochemical measurement. Protein G−HRP was purchased from Genescript. A pooled healthy human serum sample was obtained from Innovative research Inc. For human serum sample preparation, different concentrations of human Tau antigen (/*β*-amyloid 42 protein/TAR-DNA binding protein) were directly spiked into pooled human serum samples and vortexed for 2 min before application for the detection test. The three-electrode sensors were fabricated by Conductive Technologies (PA, USA). The sensor is fabricated on a polyethylene terephthalate substrate through a vapor-deposited gold working and counter electrode with a working electrode surface area of 1.54 mm^2 and a thick film printed Ag/AgCl as the reference electrode.

Biosensor Preparation and DPV Detection Procedure. The gold sensor arrays were first cleaned based on a previous reported procedure.[20] The bioconjugated Tau antibody (13 μL, 0.8 nM) in 0.1 M PBS solution (with 25 mM EDTA and 25 mM NaCl) was applied onto the gold sensor arrays for incubation of 90 min. After incubation, the biosensors were cleaned by immersing in 0.1 M PBS solution for 1 min and dried gently by nitrogen gas. The spiked Tau protein samples (18 μL) were then directly applied onto the biosensors for incubation along with the addition of 2 μL of 1 μM protein-G in 0.1 M PBS solution (100 nM of protein G) into the incubation solution. Five minutes incubation period was applied for the PBS sample, and 10 min incubation period was applied for the human serum sample. After sample incubation, the biosensors were then immersed into 0.1 M PBS solution for cleaning and dried gently by nitrogen gas after cleaning and ready for test. Differential pulse voltammetry was applied for detection with the presence of 20 μL of 0.5 mM of $[Fe(CN)_6]^{3-/4-}$ in 0.1 M PBS solution with a potential step of 0.004 V, pulse period of 0.2 s, pulse amplitude of 0.05 V, and pulse width of 0.05 s.

Amperometric Detection by HRP/HQ/H_2O_2. To quantify surface-immobilized HRP−protein G concentration, amperometric *i*−*t* was applied at −0.2 V (vs Ag/AgCl) with a 20 μL of 0.1 M HQ in 0.1 M PBS solution (prepared freshly before the test. Color change and loss of activity were observed for storage of HQ solution over 1 day.) firstly added onto the gold sensor. After 10 s, a stabilized current was observed, and 2 μL of 2 M H_2O_2 solution in deionized water was then added into the HQ solution. After the addition of H_2O_2 solution, immediate current drop was observed, and the peak of the current drop was used as the quantification signal.

ASSOCIATED CONTENT

Supporting Information

The Supporting Information is available free of charge at https://pubs.acs.org/doi/10.1021/acssensors.9b01902.

Bioconjugation modification of antibody; electrochemical impedance spectroscopy; differential pulse voltammetry evaluation of antibody concentration in acidic pH; biomolecular surface density evaluation by cathodic stripping analysis; differential pulse voltammetry detection of Tau antigen (demonstration of charge accumulated); comparison of signal outputs on Tau detection in different matrixes based on 5 min incubation of sample; evaluation of the selectivity for Tau detection; and evaluation of the matrix effect for enzymatic quantification (PDF)

AUTHOR INFORMATION

Corresponding Author

*E-mail: cxl9@case.edu.

ORCID

Yifan Dai: 0000-0002-1009-5790

Chung Chiun Liu: 0000-0002-4313-8064

Author Contributions

Y.D. conceived the idea and designed the experiments. W.X., Y.D. conducted the experiments. The manuscript was written through contributions of all authors. All authors have given approval to the final version of the manuscript.

Notes

The authors declare no competing financial interest.

ACKNOWLEDGMENTS

We gratefully appreciate the experimental supports from Electronics Design Center and the funding support from Wallace R. Persons Research Fund from Case Alumni Association.

REFERENCES

(1) Wang, G.; Das, J.; Ahmed, S.; Nemr, C. R.; Zhang, L.; Poudineh, M.; Sargent, E. H.; Kelley, S. O. Curvature-Mediated Surface Accessibility Enables Ultrasensitive Electrochemical Human Methyltransferase Analysis. *ACS Sens.* **2018**, *3*, 1765−1772.

(2) Vallée-Bélisle, A.; Ricci, F.; Uzawa, T.; Xia, F.; Plaxco, K. W. Bioelectrochemical Switches for the Quantitative Detection of Antibodies Directly in Whole Blood. *J. Am. Chem. Soc.* **2012**, *134*, 15197−15200.

(3) Draisma, G.; Etzioni, R.; Tsodikov, A.; Mariotto, A.; Wever, E.; Gulati, R.; Feuer, E.; de Koning, H. Lead time and overdiagnosis in prostate-specific antigen screening: importance of methods and context. *J. Natl. Cancer Inst.* **2009**, *101*, 374−383.

(4) Papadopulos-Eleopulos, E.; Turner, V. F.; Papadimitriou, J. M. Is a positive Western Blot proof of HIV infection? *Nat. Biotechnol.* **1993**, *11*, 696−707.

DOI: 10.1021/acssensors.9b01902
ACS Sens. 2020, 5, 140−146

(5) Kim, J.; Campbell, A. S.; de Ávila, B. E.-F.; Wang, J. Wearable biosensors for healthcare monitoring. *Nat. Biotechnol.* **2019**, *37*, 389−406.
(6) Dai, Y.; Liu, C. C. Recent Advances on Electrochemical Biosensing Strategies toward Universal Point-of-Care Systems. *Angew. Chem., Int. Ed.* **2019**, *58*, 12355−12368.
(7) Ito, Y.; Okuda-Shimazaki, J.; Tsugawa, W.; Loew, N.; Shitanda, I.; Lin, C.-E.; La Belle, J.; Sode, K. Third generation impedimetric sensor employing direct electron transfer type glucose dehydrogenase. *Biosens. Bioelectron.* **2019**, *129*, 189−197.
(8) Lee, I.; Loew, N.; Tsugawa, W.; Ikebukuro, K.; Sode, K. Development of a third-generation glucose sensor based on the open circuit potential for continuous glucose monitoring. *Biosens. Bioelectron.* **2019**, *124*−*125*, 216−223.
(9) Lee, J.; Yoshida, W.; Abe, K.; Nakabayashi, K.; Wakeda, H.; Hata, K.; Marquette, C. A.; Blum, L. J.; Sode, K.; Ikebukuro, K. Development of an electrochemical detection system for measuring DNA methylation levels using methyl CpG-binding protein and glucose dehydrogenase-fused zinc finger protein. *Biosens. Bioelectron.* **2017**, *93*, 118−123.
(10) Campuzano, S.; Serafín, V.; Gamella, M.; Pedrero, M.; Yáñez-Sedeño, P.; Pingarrón, J. M. Opportunities, Challenges, and Prospects in Electrochemical Biosensing of Circulating Tumor DNA and Its Specific Features. *Sensors* **2019**, *19*, 3762.
(11) Das, J.; Ivanov, I.; Safaei, T. S.; Sargent, E. H.; Kelley, S. O. Combinatorial Probes for High-Throughput Electrochemical Analysis of Circulating Nucleic Acids in Clinical Samples. *Angew. Chem., Int. Ed.* **2018**, *57*, 3711−3716.
(12) Zhu, Y.; Jović, M.; Lesch, A.; Tissières Lovey, L.; Prudent, M.; Pick, H.; Girault, H. H. Immuno-affinity amperometric detection of bacterial infections. *Angew. Chem., Int. Ed.* **2018**, *57*, 14942−14946.
(13) Wan, Y.; Zhou, Y.-G.; Poudineh, M.; Safaei, T. S.; Mohamadi, R. M.; Sargent, E. H.; Kelley, S. O. Highly Specific Electrochemical Analysis of Cancer Cells using Multi-Nanoparticle Labeling. *Angew. Chem., Int. Ed.* **2014**, *53*, 13145−13149.
(14) Mahshid, S. S.; Camiré, S.; Ricci, F.; Vallée-Bélisle, A. A Highly Selective Electrochemical DNA-Based Sensor That Employs Steric Hindrance Effects to Detect Proteins Directly in Whole Blood. *J. Am. Chem. Soc.* **2015**, *137*, 15596−15599.
(15) Mahshid, S. S.; Ricci, F.; Kelley, S. O.; Vallée-Bélisle, A. Electrochemical DNA-Based Immunoassay That Employs Steric Hindrance To Detect Small Molecules Directly in Whole Blood. *ACS Sens.* **2017**, *2*, 718−723.
(16) Zhou, W.; Mahshid, S. S.; Wang, W.; Vallée-Bélisle, A.; Zandstra, P. W.; Sargent, E. H.; Kelley, S. O. Steric Hindrance Assay for Secreted Factors in Stem Cell Culture. *ACS Sens.* **2017**, *2*, 495−500.
(17) Mahshid, S. S.; Mahshid, S.; Vallée-Bélisle, A.; Kelley, S. O. Peptide-Mediated Electrochemical Steric Hindrance Assay for One-Step Detection of HIV Antibodies. *Anal. Chem.* **2019**, *91*, 4943−4947.
(18) Björck, L.; Kronvall, G. Purification and some properties of streptococcal protein G, a novel IgG-binding reagent. *J. Immunol.* **1984**, *133*, 969−974.
(19) Gronenborn, A.; Filpula, D.; Essig, N.; Achari, A.; Whitlow, M.; Wingfield, P.; Clore, G. A novel, highly stable fold of the immunoglobulin binding domain of streptococcal protein G. *Science* **1991**, *253*, 657−661.
(20) Dai, Y.; Wang, C.; Chiu, L.-Y.; Abbasi, K.; Tolbert, B. S.; Sauvé, G.; Yen, Y.; Liu, C.-C. Application of bioconjugation chemistry on biosensor fabrication for detection of TAR-DNA binding protein 43. *Biosens. Bioelectron.* **2018**, *117*, 60−67.
(21) Cohen, T. J.; Friedmann, D.; Hwang, A. W.; Marmorstein, R.; Lee, V. M. Y. The microtubule-associated tau protein has intrinsic acetyltransferase activity. *Nat. Struct. Mol. Biol.* **2013**, *20*, 756−762.
(22) Min, S.-W.; Chen, X.; Tracy, T. E.; Li, Y.; Zhou, Y.; Wang, C.; Shirakawa, K.; Minami, S. S.; Defensor, E.; Mok, S. A.; Sohn, P. D.; Schilling, B.; Cong, X.; Ellerby, L.; Gibson, B. W.; Johnson, J.; Krogan, N.; Shamloo, M.; Gestwicki, J.; Masliah, E.; Verdin, E.; Gan, L. Critical role of acetylation in tau-mediated neurodegeneration and cognitive deficits. *Nat. Med.* **2015**, *21*, 1154−1162.
(23) Dai, Y.; Chiu, L.-Y.; Chen, Y.; Qin, S.; Wu, X.; Liu, C. C. Neutral Charged Immunosensor Platform for Protein-based Biomarker Analysis with Enhanced Sensitivity. *ACS Sens.* **2019**, *4*, 161−169.
(24) Povedano, E.; Valverde, A.; Montiel, V. R. V.; Pedrero, M.; Yáñez-Sedeño, P.; Barderas, R.; San Segundo-Acosta, P.; Peláez-García, A.; Mendiola, M.; Hardisson, D.; Campuzano, S.; Pingarrón, J. M. Rapid Electrochemical Assessment of Tumor Suppressor Gene Methylations in Raw Human Serum and Tumor Cells and Tissues Using Immunomagnetic Beads and Selective DNA Hybridization. *Angew. Chem.* **2018**, *130*, 8326−8330.
(25) Patel, S. P.; Kurzrock, R. PD-L1 expression as a predictive biomarker in cancer immunotherapy. *Mol. Cancer Ther.* **2015**, *14*, 847−856.
(26) Yang, W.; Justin Gooding, J.; Brynn Hibbert, D. Characterisation of gold electrodes modified with self-assembled monolayers of L-cysteine for the adsorptive stripping analysis of copper. *J. Electroanal. Chem.* **2001**, *516*, 10−16.
(27) Chen-Plotkin, A. S.; Lee, V. M.-Y.; Trojanowski, J. Q. TAR DNA-binding protein 43 in neurodegenerative disease. *Nat. Rev. Neurol.* **2010**, *6*, 211−220.
(28) Bitan, G.; Kirkitadze, M. D.; Lomakin, A.; Vollers, S. S.; Benedek, G. B.; Teplow, D. B. Amyloid β-protein (Aβ) assembly: Aβ40 and Aβ42 oligomerize through distinct pathways. *Proc. Natl. Acad. Sci. U.S.A.* **2003**, *100*, 330−335.
(29) Citron, M.; Westaway, D.; Xia, W.; Carlson, G.; Diehl, T.; Levesque, G.; Johnson-Wood, K.; Lee, M.; Seubert, P.; Davis, A.; Kholodenko, D.; Motter, R.; Sherrington, R.; Perry, B.; Yao, H.; Strome, R.; Lieberburg, I.; Rommens, J.; Kim, S.; Schenk, D.; Fraser, P.; St George Hyslop, P.; Selkoe, D. J. Mutant presenilins of Alzheimer's disease increase production of 42-residue amyloid β-protein in both transfected cells and transgenic mice. *Nat. Med.* **1997**, *3*, 67−72.
(30) Ruiz-Valdepeñas Montiel, V.; Povedano, E.; Vargas, E.; Torrente-Rodríguez, R. M.; Pedrero, M.; Reviejo, A. J.; Campuzano, S.; Pingarrón, J. M. Comparison of Different Strategies for the Development of Highly Sensitive Electrochemical Nucleic Acid Biosensors Using Neither Nanomaterials nor Nucleic Acid Amplification. *ACS Sens.* **2018**, *3*, 211−221.

DOI: 10.1021/acssensors.9b01902
ACS Sens. 2020, 5, 140−146